HHS Public Access

Author manuscript

Cytoskeleton (Hoboken). Author manuscript; available in PMC 2018 September 01.

Published in final edited form as:

Cytoskeleton (Hoboken). 2017 September ; 74(9): 356–366. doi:10.1002/cm.21386.

Native Kinesin-1 Does Not Bind Preferentially to GTP-Tubulin-Rich Microtubules In Vitro

Qiaochu Li[1], **Stephen J. King**[2], and **Jing Xu**[1,*]

[1]Department of Physics, University of California, Merced, CA 95343, USA

[2]Burnett School of Biomedical Sciences, University of Central Florida, FL 32827, USA

Abstract

Molecular motors such as kinesin-1 work in small teams to actively shuttle cargos in cells, for example in polarized transport in axons. Here we examined the potential regulatory role of the nucleotide state of tubulin on the run length of cargos carried by multiple kinesin motors, using an optical trapping-based in vitro assay. Based on a previous report that kinesin binds preferentially to GTP-tubulin-rich microtubules, we anticipated that multiple-kinesin cargos would run substantially greater distances along GMPCPP microtubules than along GDP microtubules. Surprisingly, we did not uncover any significant differences in run length between microtubule types. A combination of single-molecule experiments, comparison with previous theory, and classic microtubule affinity pulldown assays revealed that native kinesin-1 does not bind preferentially to GTP-tubulin-rich microtubules. The apparent discrepancy between our observations and the previous report likely reflects differences in post-translational modifications between the native motors used here and the recombinant motors examined previously. Future investigations will help shed light on the interplay between the motor's post-translational modification and the microtubule's nucleotide-binding state for transport regulation in vivo.

Keywords

Optical trap; Multiple Motor Transport; GMPCPP; GDP; Tubulin Nucleotide State

Introduction

Molecular motor-based transport is critical for the function and survival of all eukaryotic cells [Hirokawa et al., 2010; Mandelkow and Mandelkow, 2002; Vale, 2003]. Molecular motors such as kinesin-1 actively step along microtubules to distribute cargo in cells. This transport process is sensitive to the run length of cargos along microtubules. Because molecular motors often work in small teams to shuttle cargos in cells [Gross et al., 2007; Hancock, 2008; Hendricks et al., 2010; Kural et al., 2005; Rai et al., 2016; Rai et al., 2013; Shubeita et al., 2008; Weaver et al., 2013], understanding the key factors impacting multiple

*Address correspondence to: Jing Xu, jxu8@ucmerced.edu.

Supplementary Material

Supplementary figures and references are included online.

motor-based transport is crucial for understanding and ultimately harnessing transport regulation in cells.

Microtubules are cytoskeletal filaments that form the “molecular highways” for motor-based transport in cells. Microtubules are polymerized from tubulin subunits. There is increasing evidence that the biochemical nature of tubulin plays a key role in regulating motor-based transport [Alper et al., 2014; Cai et al., 2009; Feizabadi et al., 2015; Garnham et al., 2015; Janke, 2014; McKenney et al., 2016; Morikawa et al., 2015; Nakata et al., 2011; Nirschl et al., 2016; Sirajuddin et al., 2014; Uchimura et al., 2010; Verhey and Gaertig, 2007; Wang and Sheetz, 2000]. In the current study, we examined the impact of the nucleotide state of the tubulin subunits within microtubules on multiple-kinesin based transport.

Our study was motivated by a previous finding that kinesin-1 preferentially binds GTP-tubulin-rich microtubules [Nakata et al., 2011]. Depending on the concentration of motors present in solution, the binding affinity of a single, cargo-free kinesin can be up to ~3.7× higher for GMPCPP microtubules (mimicking GTP-tubulin [Hyman et al., 1992]) than for GDP microtubules [Morikawa et al., 2015; Nakata et al., 2011]. This effect was proposed to underlie polarized transport in axons [Nakata et al., 2011], by promoting preferential loading of kinesin-based cargos onto the axon initial segment, where microtubules are enriched in GTP-tubulin [Nakata et al., 2011]. Because binding affinity is a key determinant of multiple-motor transport [Klumpp and Lipowsky, 2005; Kunwar et al., 2008] (Fig. S1), we anticipated that the run length of multiple-kinesin cargos would be significantly longer for GMPCPP microtubules than for GDP microtubules. Such a run-length increase in the kinesin-based anterograde direction has the potential to further promote polarized transport in axons.

Here, we used optical trap-based biophysical studies to test the hypothesis that the run length of multiple-kinesin cargos is enhanced for GTP-tubulin-rich microtubules. As in previous work [Nakata et al., 2011], we used GMPCPP microtubules to model microtubules enriched with GTP-tubulin, as well as standard GDP microtubules as controls. We verified that GMPCPP microtubules are stable at room temperature without the stabilizing agent taxol (Supporting Text and Fig. S2). Because the presence of an oligo-histidine tag has been shown to significantly increase the binding affinity of the end-binding protein EB1 for GMPCPP microtubules [Maurer et al., 2011; Zhu et al., 2009], we focused on native kinesin motors lacking affinity purification tags. To purify the tagless, native kinesin motor, we employed the classic microtubule-affinity-based purification method [Schroer and Sheetz, 1991], with the exception that 9S kinesin was eluted from the Mono-Q resin using a series of customized salt gradients to isolate the motor from other polypeptides in the 9S sucrose fractions [Li et al., 2016; Vershinin et al., 2007]. We used standard polystyrene beads as our in vitro cargos [Gelles et al., 1988] to quantify multiple-kinesin run length, and controlled the range of motor number per cargo as we did previously [Li et al., 2016; Liang et al., 2016; Xu et al., 2013; Xu et al., 2012b] (Fig. S3). Note that binding of native kinesin-1 to the in vitro cargo relieves the motor from tail-mediated autoinhibition and enables motor-based cargo motility [Coy et al., 1999; Friedman and Vale, 1999].

Surprisingly, we did not detect a significant difference in the run lengths of multiple-kinesin cargos between GMPCPP microtubules and GDP microtubules. Our single-motor measurements also demonstrated similar dissociation rates and velocities for both microtubule types. Combined, our data suggest that kinesin has similar binding rates for both microtubule types. To test the validity of this surprising, biophysics-based finding, we biochemically probed the binding affinity of the native motor using a classical microtubule-affinity pulldown assay [Huang and Hackney, 1994]. Our pulldown data confirmed that native kinesin-1 does not preferentially bind microtubules enriched in GTP-tubulin.

Results and Discussion

The presence of taxol does not impact the motility of multiple-kinesin cargos along GMPCPP microtubules

We first controlled for the potential effect of taxol on cargo transport along GMPCPP microtubules (Fig. 1). Although taxol is not needed to stabilize GMPCPP microtubules, it is necessary to stabilize GDP microtubules (Fig. S2A). Previous studies indicated that the presence of taxol does not influence the motility (run length or velocity) of single kinesins along GMPCPP microtubules [McVicker et al., 2011], nor does taxol influence the multiple kinesin-based gliding velocity of GMPCPP microtubules in vitro [LaPointe et al., 2013]. However, these previous investigations used truncated kinesin-1 constructs, not the native kinesin-1 employed here. We carried out parallel motility experiments using identical, taxol-free preparations of GMPCPP microtubules and kinesin/bead complexes, while varying the taxol content in buffers used in flow-cell preparation and subsequent motility experiments (0 μM or 25 μM, Fig. 1).

We focused our investigations on transport by an average of ~2 kinesins per cargo, which matches the range reported for kinesin-based cargos in vivo [Hendricks et al., 2010; Shubeita et al., 2008]. Although quantitative control over motor number per cargo remains an active area of research, we and others previously characterized the run length of cargos carried by exactly two kinesins (via DNA- or protein-based assembly; [Derr et al., 2012; Furuta et al., 2013; Norris et al., 2014; Rogers et al., 2009; Xu et al., 2012b]). Specifically, we and others demonstrated that the average run length of two-kinesin cargos is ~1.7× longer than the single-kinesin value [Rogers et al., 2009; Xu et al., 2012b]. Here, we used this known scaling of two-kinesin run length as a “scale bar”, and empirically tuned the kinesin/bead ratio such that the resulting cargo run length displayed a similar increase from the single-kinesin value (Fig. S3).

We did not detect any significant effect of taxol on cargo run length along GMPCPP microtubules (Fig. 1A). Although the mean run length along taxol-free GMPCPP microtubules was somewhat shorter than that in the presence of taxol (1 μm vs. 1.17 μm, Fig. 1A(i)), this difference was not statistically significant ($P = 0.60$, rank-sum test, Fig. 1A(ii)). The lack of difference in cargo run length was evident when we contrasted the cumulative probability distributions of the same measurements (Fig. 1A(ii)). For longer run lengths, the cumulative probability distribution also highlighted subtle deviations from a single exponential (scatter vs. line, Fig. 1A(ii)). Deviation from a single exponential is expected for multiple-motor measurements, whose distribution is better approximated by a

sum of multiple single exponentials [Beeg et al., 2008; Klumpp and Lipowsky, 2005]. Importantly for the current study, such deviation does not impact our ability to determine the significance of differences between measurements using the rank-sum test ($P = 0.60$, Fig. 1A(ii)). We also did not detect any significant effect of taxol on the transport velocity of cargos along GMPCPP microtubules ($P = 0.82$, Student's *t*-test, Fig. 1B). These results are in excellent agreement with previous studies of truncated kinesin-1 constructs in single-motor motility assays [McVicker et al., 2011] or microtubule gliding assays [LaPointe et al., 2013].

Taken together, our data demonstrate that the presence of taxol in motility experiments does not influence kinesin-based motility on GMPCPP microtubules.

The run length of multiple-kinesin cargos does not differ significantly between GMPCPP and GDP microtubules

We next carried out parallel comparisons of multiple-kinesin run length along GMPCPP microtubules and GDP microtubules (Fig. 2). To eliminate potential variations in kinesin/bead ratio between preparations, we used a single kinesin/bead preparation for each set of pairwise comparisons between microtubule types. Because the presence of taxol does not impact kinesin-based cargo motility along GMPCPP microtubules (Fig. 1, and [LaPointe et al., 2013; McVicker et al., 2011]), we included taxol in our kinesin/bead preparations as well as in all buffers used in our motility experiments.

Surprisingly, we did not detect any significant difference in the run length of ~two-kinesin cargos between microtubule types ($P = 0.60$, rank-sum test, Fig. 2A(i)). For this set of measurements, we used the same kinesin/bead ratio as in Figure 1 (~two-kinesin transport range, Fig. S3). We speculated that more motors may be necessary to achieve the difference in run length that we predicted. In principle, the more motors present on a cargo, the greater the cumulative effect of a change at the single-motor level (such as increased binding affinity) on overall cargo transport. To test this possibility, we increased the average number of motors per cargo by tuning up the kinesin/bead ratio in our experiments. As a result, the associated cargo run length increased substantially (from 1.38 μm in Fig. 2A(i) to 3.31 μm in Fig. 2A(iii), GDP microtubules). The deviation of measurements from a single exponential at the longer run lengths became more pronounced (scatter vs. line, Fig. 2A), again indicating an increase in the number of motors per cargo. At the highest kinesin/bead ratio, the average run length was 4.4× longer than that of single-motor transport (GDP microtubules, 3.31 μm in Fig. 2A(iii) vs. 0.75 μm in Fig. S3B). This extended run length corresponds to transport mediated by ~3–4 motors per cargo, based on previous investigations of transport by a well-defined number of kinesin motors [Derr et al., 2012; Furuta et al., 2013; Norris et al., 2014]. We did not further increase the kinesin/bead ratio, because the differential binding effect diminishes at higher motor concentrations [Morikawa et al., 2015; Nakata et al., 2011]. Nonetheless, despite a substantial increase in the number of motors per cargo, we did not detect any significant difference in cargo run length between microtubule types (for example, Fig. 2A). The mean run lengths for each pairwise comparison agreed well with each other (within 12%, Fig. 2B). The corresponding distributions of run length also did not differ significantly from each other ($P \geq 0.40$, rank-

sum test, Fig. 2B). Thus, in contrast to our prediction, the run length of multiple-kinesin cargos is not significantly enhanced along GTP-tubulin-rich microtubules.

The dissociation rate of a single kinesin does not differ between GMPCPP and GDP microtubules

To understand the lack of difference in multiple-kinesin run length (Fig. 2), we sought to determine whether the dissociation rate of a single kinesin differs between microtubule types. The run length of multiple-motor cargos is sensitive to the motor's dissociation rate as well as its binding rate [Klumpp and Lipowsky, 2005; Kunwar et al., 2011; Kunwar et al., 2008; Ori-McKenney et al., 2010; Xu et al., 2012b] (Fig. S1). The null effect on multiple-motor run length in Figure 2 may reflect compensatory effects between changes in the motor's binding and dissociation rates for GTP-tubulin-rich microtubules. Whereas a substantial increase in the motor's binding rate can significantly improve multiple-motor run length, this effect may be countered by a similar increase in the motor's dissociation rate.

We carried out single-molecule measurements to determine the average association time between single-kinesin cargos and microtubules. We then used the reciprocal of this association time to determine the dissociation rate. We continued to use polystyrene beads as in vitro cargos, as in classic single-molecule experiments [Block et al., 1990; Gelles et al., 1988]. To reach the single-motor range, we limited the kinesin/bead ratio such that <20% of the beads displayed motility along microtubules. We and others have previously demonstrated that, for a motile fraction <20%, most motile beads (>95%) are carried by a single kinesin [Block et al., 1990; Li et al., 2016]. For consistency, we again included taxol in all buffers in our motility experiments for both microtubule types.

We did not detect any significant difference in kinesin's association time between microtubule types ($P = 0.50$, rank-sum test, Fig. 3A). The mean association time remained ~1 s for both microtubule types (Fig. 3A), giving rise to a dissociation rate of ~1 s^{-1} for both microtubule types (Fig. 3B). It is important to note that kinesin's dissociation rate may be different in a multi-motor context, as associated motors on the cargo may influence the microtubule's interaction with dissociated motors on the same cargo. Nonetheless, our data indicate that the single-kinesin dissociation rate is not substantially influenced by the nucleotide state of tubulin. Thus, the lack of difference in multiple-kinesin run length (Fig. 2) is unlikely to result from compensatory changes in the motor's binding and dissociation rates for different microtubule types.

Comparison with theory suggests that the single-kinesin binding rate is similar for GMPCPP and GDP microtubules

We next referred to previous theoretical work [Klumpp and Lipowsky, 2005] in order to examine the possibility that parameters other than single-motor dissociation rate underlie our null finding in Figure 2. Although this previous model does not consider force-based interactions between individual motors, for kinesin-based transport, this model's predictions are in good agreement with results from stochastic simulations that include force-based interactions between motors [Kunwar et al., 2011] as well as with results from previous experimental studies employing GDP microtubules [Beeg et al., 2008; Xu et al., 2012b].

Four key parameters are highlighted to impact cargo run length in previous theoretical work [Klumpp and Lipowsky, 2005]: motor number, single-motor binding rate, single-motor dissociation rate, and single-motor velocity. Because we used the same kinesin/bead preparation to contrast between microtubule types, the number of motors available for transport did not differ between GMPCPP and GDP microtubules. We also detected very similar transport velocities of single kinesins along both microtubule types ($P = 0.15$, Student's *t*-test, Fig. 4), as did a previous single-motor study using a truncated kinesin dimer [McVicker et al., 2011]. Note that we detected a modest (~7%) but significant velocity difference in our multiple-kinesin measurements ($P = 0.004$, Student's *t*-test, Fig. 5), consistent with previous multiple kinesin-based investigations of microtubule gliding velocities (~30% faster for GMPCPP vs. GDP microtubules) [Morikawa et al., 2015; Vale et al., 1994] and suggesting a potential effect of motor number on cargo velocity.

Given that motor number, single-motor velocity, and single-motor dissociation rate are very similar between microtubule types, the binding rates of the motor should be very similar as well. However, this prediction is inconsistent with previous reports that kinesin preferentially binds GMPCPP versus GDP microtubules [Morikawa et al., 2015; Nakata et al., 2011]. It is possible that measurement uncertainties for individual parameters may combine to obscure a substantial effect of the motor's binding affinity on cargo run length. It is also possible that the force-based interaction between motors (not included in the theoretical model) could be altered by the nucleotide state of tubulin in microtubules. Lastly, although extensive in vitro studies suggest that this is unlikely [Block et al., 1990; Gelles et al., 1988; Xu et al., 2012a], it is formally possible that polystyrene beads may alter the interactions between the motor and the microtubule in unexpected ways. Since it is challenging to completely rule out these potential concerns in biophysics-based assays, we next turned to a biochemistry-based assay.

Native kinesin-1 does not preferentially co-sediment with GTP-tubulin-rich microtubules

To overcome the uncertainties associated with our biophysical assays, we employed the classic microtubule affinity pulldown assay [Huang and Hackney, 1994] to biochemically probe the binding of native kinesin-1 to microtubules (Fig. 6). Results from this co-sedimentation assay are bead-independent and free from considerations of force-based interaction between motors. Briefly, we incubated kinesins with microtubules, prior to pelleting the microtubules and quantifying the co-sedimentation of kinesin with pellets of different microtubule types. Note that kinesin's tail does not prevent the motor from binding microtubules [Coy et al., 1999; Friedman and Vale, 1999]. Because differential binding was most pronounced for 10–100 nM kinesin [Morikawa et al., 2015; Nakata et al., 2011], we used a similar dilute kinesin concentration in our co-sedimentation assay (67 nM). To further enable direct comparison with previous measurements of kinesin's binding affinity [Nakata et al., 2011], we included taxol in co-sedimentation assays using GDP microtubules but not GMPCPP microtubules.

We examined the co-sedimentation of kinesins with microtubules at three microtubule concentrations (0.28, 0.37, and 1.1 μM, Fig. 6). For each microtubule concentration, we carried out parallel co-sedimentation assays that differed in the presence of ATP or the non-

hydrolyzable ATP analog AMPPNP (for example, Fig. 6A), in order to differentiate between relative contributions to kinesin/microtubule binding through kinesin's tail (independent of ATP, [Seeger and Rice, 2010]) versus its motor domain (dependent on ATP). We carried out gel-based protein quantitation using infrared fluorescence of Commassie-stained gels. The subunits of our purified kinesin and tubulin proteins separated well on protein gels (Fig. S4). The infrared fluorescence response of Coomassie blue is quantitative for protein content between 10 ng and 20 μg per band [Luo et al., 2006], which encompasses the range in protein content examined here (80–320 ng kinesin or 1–4 μg tubulin per lane, Fig. 6A).

For each microtubule concentration tested, we did not detect any significant difference in kinesin signals between microtubule types in assays using AMPPNP (green solid circles vs. magenta solid circles, Fig. 6B; $P > 0.57$, Student's *t*-test) or ATP (green open circles vs. magenta open circles, Fig. 6B; $P > 0.20$, Student's *t*-test). In contrast, within each microtubule type, we detected substantially higher co-sedimentation of kinesin with microtubules in the presence of AMPPNP than in the presence of ATP (Fig. 6). For example, we detected >1.8× higher kinesin signal in the pellet of GDP microtubules in assays using AMPPNP versus ATP (green solid circles vs. green open circles, Fig. 6B). Note that the presence of ATP does not completely eliminate the equilibrium association of kinesin with the microtubule through its motor domain. Thus, the majority of kinesin signal in assays using AMPPNP corresponds to the ATP-dependent binding of kinesin's motor domain to the microtubule. This observation is perhaps not surprising, as the native kinesin protein used in the current study is a holoenzyme, containing both the kinesin heavy chain and kinesin light chains (Fig. S4). Previous work [Wong and Rice, 2010] demonstrated that kinesin light chains inhibit the association of kinesin's tail with the microtubule. Taken together, our co-sedimentation data again demonstrate that native kinesin-1 does not bind preferentially to GTP-tubulin-rich microtubules.

In summary, our biophysical and biochemical data indicate that the in vitro function of native kinesin-1 does not differ substantially between GMPCPP microtubules and GDP-microtubules (Figs. 1–5). We did not detect any difference in the co-sedimentation of native kinesin with the two microtubule types (Fig. 6), as reported previously for recombinant truncated kinesin [Morikawa et al., 2015; Nakata et al., 2011]. However, we do not rule out the possibility that the tubulin-nucleotide state of microtubules plays an important role in regulating kinesin-based transport in vivo. The native kinesin examined here contains important post-translational modifications (for example, phosphorylation [Hollenbeck, 1993; Sato-Yoshitake et al., 1992]) that are absent from recombinant proteins. The apparent discrepancy between the current study and previous investigations may reflect regulation of kinesin/microtubule interactions via post-translational modification of the motor. Future investigations will help shed light on the interplay between the motor's post-translational modifications and the microtubule's nucleotide-binding state for transport regulation in vivo.

Materials and Methods

Proteins and reagents

Bovine brain tubulin was purified over a phosphocellulose column as previously described [Sloboda and Rosenbaum, 1982]. Tubulin was free of GTP prior to the phosphocellulose

column purification. The column buffer was equilibrated with 0.1 mM GTP to prevent denaturing of the purified tubulin. Rhodamine-labeled tubulin (TL590M) was purchased from Cytoskeleton Inc.

Kinesin-1 was purified from bovine brain as previously described [Schroer and Sheetz, 1991], except that 9S kinesin was eluted from the Mono-Q resin using customized salt gradients to separate kinesin from other polypeptides in the 9S sucrose fractions [Vershinin et al., 2007].

Unless otherwise specified, chemicals were purchased from Sigma-Aldrich. GMPCPP was purchased from Jena Biosciences.

Microtubule preparation

To assemble GDP microtubules, purified tubulin was diluted to 40 μM in PM buffer (100 mM PIPES, 1 mM $MgSO_4$, 2 mM EGTA, pH 6.9) supplemented with 0.5 mM GTP. This tubulin solution was incubated at 37 °C for 20 min for assembly. The assembled microtubules were mixed with an equal volume of PM buffer supplemented with 40 μM taxol, followed by a second incubation at 37 °C for 20 min. After assembly, GDP microtubules were kept at room temperature in a dark box and used within four days of preparation.

To assemble GMPCPP microtubules, purified tubulin was diluted to 4 μM in PM buffer supplemented with 1 mM GMPCPP. The resulting tubulin solution contained 125× excess of GMPCPP (1 mM) to GTP (8 μM). Because the affinity of tubulin for GMPCPP is >1/8 of its affinity for GTP [Hyman et al., 1992], we estimate that the resulting microtubules were enriched in GMPCPP tubulin (>15× excess over GDP tubulin). The tubulin solution was incubated at 37 °C for 0.5 h or 2.5 h for assembly. The shorter condition was used in tests of the stability of GMPCPP microtubules. The microtubules were then kept at room temperature and in a dark box for up to 80 h. The longer condition was used to achieve longer GMPCPP microtubules for motility measurements. With the exception of the stability test, GMPCPP microtubules were freshly prepared each day and used immediately following preparation.

For epifluorescence-based length quantification, both types of microtubules were fluorescently labeled at a ratio of 1:10 rhodamine-labeled tubulin:unlabeled tubulin.

Quantification of microtubule length

The length of microtubules was used as a readout for microtubule stability under different conditions. Measurements were carried out in standard flow cells that were prepared identically for different microtubule conditions. To construct each flow cell, we sandwiched a coverslip (22×40 mm, No. 1.5, Thermo Fisher Scientific) and a microscope slide (25×75 mm, Thermo Fisher Scientific) using double-sided tape. The coverslip and the microscope slide were biologically clean. Kinesin was diluted to 65 nM in PMEE buffer (35 mM PIPES, 5 mM $MgSO_4$, 1 mM EGTA, 0.5 mM EDTA, pH 7.2) and then introduced to the flow cell for 10 min to undergo nonspecific binding to the flow-cell surface. Casein (5.55 mg/mL in PMEE buffer) was introduced to the flow cell for 10 min to wash out excess unbound motors

and to block the flow-cell surface. Microtubules (GMPCPP or GDP) were diluted in PMEE buffer (supplemented with 0 μM taxol or 50 μM taxol as indicated), introduced to the flow cell for 10 min, and imaged at 100× magnification via epifluorescence microscopy (Eclipse Ti-E, Nikon; and iXon electron multiplier CCD, Andor). Images were exported from Nikon Elements as .tif files and imported into MatLab (MathWorks) for analysis. Microtubule length was quantified to ~10 nm resolution using Fluorescence Image Evaluation Software for Tracking and Analysis (FIESTA, version 1.05.0005) [Ruhnow et al., 2011].

Optical trapping-based motility assay

In vitro motility experiments were carried out in flow cells, which were prepared identically for GDP and GMPCPP microtubules. Flow cells were constructed as above, except that the coverslip was plasma cleaned [Gutiérrez-Medina and Block, 2010], incubated with poly-L-lysine (0.00027% w/v in ethanol, 12 min), and oven dried (85 °C, 12 min) before flow-cell construction.

To make flow cells with GDP microtubules, GDP microtubules were diluted to 140 nM in PMEE buffer supplemented with 1 mM GTP and 25 μM taxol, and then introduced to the flow cell for 10 min to undergo nonspecific binding to the poly-L-lysine-treated coverslip surface. The flow cell was rinsed with wash buffer (11.7 mM PIPES, 1.6 mM $MgSO_4$, 0.3 mM EGTA, 0.12 mM EDTA, pH 7.2) supplemented with 1 mM GTP and 25 μM taxol, and blocked with 5.55 mg/mL casein in PMEE buffer supplemented with 1 mM GTP and 25 μM taxol.

To make flow cells with GMPCPP microtubules, we used the same procedures as above, except that the GMPCPP microtubules were diluted to 40 nM and GTP was excluded from all buffers. Buffers contained 0 μM or 25 μM taxol as indicated.

For the multiple-motor measurements (Figs. 1, 2, and 5), kinesin (2.5–3.3 nM) was incubated with carboxylated polystyrene beads (4.5×10^6 particles/μL, 200 nm diameter, Polysciences) in motility buffer (67 mM PIPES, 50 mM CH_3CO_2K, 3 mM $MgSO_4$, 1 mM dithiothreitol, 0.84 mM EGTA, 0 μM or 25 μM taxol as indicated, pH 6.9) for 10 min at room temperature; this solution was supplemented with an oxygen-scavenging solution (250 μg/mL glucose oxidase, 30 μg/mL catalase, 4.6 mg/mL glucose) and 1 mM ATP prior to motility measurements. For example, we incubated 4.5×10^6 beads/μL with 2.5 nM (Fig. 2Ai), 2.9 nM (Fig. 2Aii), and 3.3 nM (Fig. 2Aiii) kinesin. We verified that cargo transport was mediated by multiple kinesins, because the average cargo run length was substantially higher than that of the single-kinesin value (Fig. S3). To eliminate potential variations in kinesin/bead ratio between preparations, we used the same kinesin/bead preparation to contrast between microtubule types and repeated our experiments 3–4 times for each set of pairwise comparisons.

For the single-motor studies (Figs. 3 and 4), kinesin (0.1–0.17 nM) was incubated with carboxylated polystyrene beads (3.6×10^5 particles/μL, 500 nm diameter, Polysciences) in motility buffer for 10 min at room temperature, supplemented with an oxygen-scavenging solution and 1 mM ATP prior to motility measurements. At this motor/bead incubation ratio,

≤20% of the motor/bead complexes exhibited motility along microtubules, and >95% of the motile events were carried by a single kinesin [Block et al., 1990; Li et al., 2016].

A single-beam optical trap was used to facilitate motility measurements as previously described [Block et al., 1990; Li et al., 2016]. We used a very weak trap power (<20 mW at fiber output), such that the trap was sufficient for positioning individual beads but could not stall beads carried by a single kinesin [Li et al., 2016]. We also turned off the optical trap upon observation of directed bead motion along the microtubule to enable cargo transport without external load.

Video recordings of bead motion (30 Hz) were particle-tracked to 10 nm resolution (1/3 pixel) using a template-matching algorithm as previously described [Carter et al., 2005].

Analysis of in vitro motility data

The run length of a motile bead was determined as the net displacement of the bead along the microtubule between landing and dissociation. To account for the time that elapsed during manual shut-off of the optical trap, only trajectories with >300 nm of motion were analyzed. For each experimental condition (kinesin/bead incubation ratio, microtubule type), the cumulative probability distribution of run length was fitted to the cumulative probability function of a single exponential distribution, $1 - Ae^{-x/d}$. Mean run length and standard error for each distribution were determined from the best-fit decay constant d and uncertainty, respectively.

To evaluate bead velocity under no load, only portions of each trajectory >300 nm were used. For each microtubule type (GDP or GMPCPP), the cumulative probability distribution of single-kinesin velocity was fitted to the cumulative probability function of a Gaussian distribution, $\frac{1}{2}\left[1+erf\left(\frac{x-v}{A}\right)\right]$. Mean velocity and standard error for each distribution were determined from the best-fit mean v and uncertainty, respectively.

The association time of a single-kinesin bead with the microtubule was determined as the time between landing and dissociation. To account for human reaction time during manual shut-off of the optical trap, only trajectories >0.3 s were analyzed. For each microtubule type, the cumulative probability distribution of the association time was fitted to the cumulative probability function of a single exponential distribution, $1 - Ae^{-x/t}$. Mean association time and standard error for each distribution were determined from the best-fit decay constant t and uncertainty, respectively.

Microtubule affinity pulldown assay

Kinesin (66 nM) was incubated with 1.1 μM GDP microtubules in PMEE buffer (supplemented with 25 μM taxol and 5 mM AMPPNP or 5 mM ATP as indicated) or ~1.7 μM GMPCPP microtubules in PMEE buffer (taxol-free, supplemented with 5 mM AMPPNP or 5 mM ATP as indicated). Assays using ATP were supplemented with an ATP-regenerating system (2 mM phosphocreatine and 70 μg/mL creatine phosphokinase) [Huang and Hackney, 1994]. Kinesin/microtubule mixtures were identically incubated at 37 °C for 25 min, followed by centrifugation in a TLS55 rotor for 10 min at 170,000 × g at 25 °C. The

resulting pellets were dissolved in 40 uL 1× reducing SDS sample buffer (Thermo Fisher Scientific), heated to 80 °C for 10 min, and separated via SDS-PAGE (4–12% Bis-Tris protein gel, NuPAGE, Thermo Fisher Scientific). Gels were imaged in near infrared (700 nm) using a commercial scanner (Odyssey, Li-Cor Biosciences).

Statistical analysis

The rank-sum test was used to detect significant differences between two distributions of run-length measurements. Student's *t*-test was used to determine the significance of differences between two distributions of velocity measurements and between two sets of co-sedimentation measurements.

Supplementary Material

Refer to Web version on PubMed Central for supplementary material.

Acknowledgments

We thank our reviewers for helpful comments, Christopher L. Berger and Keir C. Neuman for helpful discussions, and Bayana Science for manuscript editing. We thank John Wilson in the Xu lab for help with microtubule length analysis using FIESTA. We thank Frederick W. Wolf for use of LI-COR Odyssey imaging system.

We acknowledge support from the UC Merced Senate Committee on Research (to J.X.), the UC Merced Startup (to J.X.), and the National Institutes of Health (NS048501 to S.J.K, R15GM120682 to J.X.).

References

Alper JD, Decker F, Agana B, Howard J. The Motility of Axonemal Dynein Is Regulated by the Tubulin Code. Biophys J. 2014; 107:2872–2880. [PubMed: 25658008]

Beeg J, Klumpp S, Dimova R, Gracia RS, Unger E, Lipowsky R. Transport of beads by several kinesin motors. Biophys J. 2008; 94:532–541. [PubMed: 17872957]

Block SM, Goldstein LS, Schnapp BJ. Bead movement by single kinesin molecules studied with optical tweezers. Nature. 1990; 348:348–352. [PubMed: 2174512]

Cai D, McEwen DP, Martens JR, Meyhofer E, Verhey KJ. Single molecule imaging reveals differences in microtubule track selection between Kinesin motors. PLoS Biol. 2009; 7:e1000216. [PubMed: 19823565]

Carter BC, Shubeita GT, Gross SP. Tracking single particles: A user-friendly quantitative evaluation. Phys Biol. 2005; 2:60–72. [PubMed: 16204858]

Conway L, Wood D, Tuzel E, Ross JL. Motor transport of self-assembled cargos in crowded environments. Proc Natl Acad Sci U S A. 2012; 109:20814–20819. [PubMed: 23213204]

Coy DL, Hancock WO, Wagenbach M, Howard J. Kinesin's tail domain is an inhibitory regulator of the motor domain. Nature Cell Biology. 1999; 1:288–292. [PubMed: 10559941]

Derr ND, Goodman BS, Jungmann R, Leschziner AE, Shih WM, Reck-Peterson SL. Tug-of-war in motor protein ensembles revealed with a programmable DNA origami scaffold. Science. 2012; 338:662–665. [PubMed: 23065903]

Feizabadi MS, Narayanareddy BRJ, Vadpey O, Jun Y, Chapman D, Rosenfeld S, Gross SP. Microtubule C-Terminal Tails Can Change Characteristics of Motor Force Production. Traffic. 2015; 16:1075–1087. [PubMed: 26094820]

Friedman DS, Vale RD. Single-molecule analysis of kinesin motility reveals regulation by the cargo-binding tail domain. Nat Cell Biol. 1999; 1:293–297. [PubMed: 10559942]

Furuta K, Furuta A, Toyoshima YY, Amino M, Oiwa K, Kojima H. Measuring collective transport by defined numbers of processive and nonprocessive kinesin motors. Proc Natl Acad Sci U S A. 2013; 110:501–506. [PubMed: 23267076]

Garnham CP, Vemu A, Wilson-Kubalek EM, Yu I, Szyk A, Lander GC, Milligan RA, Roll-Mecak A. Multivalent Microtubule Recognition by Tubulin Tyrosine Ligase-like Family Glutamylases. Cell. 2015; 161:1112–1123. [PubMed: 25959773]

Gelles J, Schnapp BJ, Sheetz MP. Tracking kinesin-driven movements with nanometre-scale precision. Nature. 1988; 331:450–453. [PubMed: 3123999]

Gross SP, Vershinin M, Shubeita GT. Cargo transport: Two motors are sometimes better than one. Current Biology. 2007; 17:R478–R486. [PubMed: 17580082]

Gutiérrez-Medina B, Block SM. Visualizing individual microtubules by bright field microscopy. Am J Phys. 2010; 78:1152–1159.

Hancock WO. Intracellular transport: kinesins working together. Curr Biol. 2008; 18:R715–717. [PubMed: 18727910]

Hendricks AG, Perlson E, Ross JL, Schroeder HW 3rd, Tokito M, Holzbaur EL. Motor coordination via a tug-of-war mechanism drives bidirectional vesicle transport. Curr Biol. 2010; 20:697–702. [PubMed: 20399099]

Hirokawa N, Niwa S, Tanaka Y. Molecular motors in neurons: Transport mechanisms and roles in brain function, development, and disease. Neuron. 2010; 68:610–638. [PubMed: 21092854]

Hollenbeck PJ. Phosphorylation of neuronal kinesin heavy and light chains in vivo. J Neurochem. 1993; 60:2265–2275. [PubMed: 8492130]

Huang TG, Hackney DD. Drosophila kinesin minimal motor domain expressed in Escherichia coli. Purification and kinetic characterization. J Biol Chem. 1994; 269:16493–16501. [PubMed: 8206959]

Hyman AA, Salser S, Drechsel DN, Unwin N, Mitchison TJ. Role of GTP hydrolysis in microtubule dynamics: information from a slowly hydrolyzable analogue, GMPCPP. Mol Biol Cell. 1992; 3:1155–1167. [PubMed: 1421572]

Janke C. The tubulin code: Molecular components, readout mechanisms, and functions. J Cell Biol. 2014; 206:461–472. [PubMed: 25135932]

Klumpp S, Lipowsky R. Cooperative cargo transport by several molecular motors. Proc Natl Acad Sci USA. 2005; 102:17284–17289. [PubMed: 16287974]

Kunwar A, Tripathy SK, Xu J, Mattson MK, Anand P, Sigua R, Vershinin M, McKenney RJ, Yu CC, Mogilner A, et al. Mechanical stochastic tug-of-war models cannot explain bidirectional lipid-droplet transport. Proc Natl Acad Sci U S A. 2011; 108:18960–18965. [PubMed: 22084076]

Kunwar A, Vershinin M, Xu J, Gross SP. Stepping, strain gating, and an unexpected force-velocity curve for multiple-motor-based transport. Curr Biol. 2008; 18:1173–1183. [PubMed: 18701289]

Kural C, Kim H, Syed S, Goshima G, Gelfand VI, Selvin PR. Kinesin and dynein move a peroxisome in vivo: A tug-of-war or coordinated movement? Science. 2005; 308:1469–1472. [PubMed: 15817813]

LaPointe NE, Morfini G, Brady ST, Feinstein SC, Wilson L, Jordan MA. Effects of eribulin, vincristine, paclitaxel and ixabepilone on fast axonal transport and kinesin-1 driven microtubule gliding: implications for chemotherapy-induced peripheral neuropathy. Neurotoxicology. 2013; 37:231–239. [PubMed: 23711742]

Li Q, King SJ, Gopinathan A, Xu J. Quantitative determination of the probability of multiple-motor transport in bead-based assays. Biophys J. 2016; 110:2720–2728. [PubMed: 27332130]

Liang WH, Li Q, Rifat Faysal KM, King SJ, Gopinathan A, Xu J. Microtubule Defects Influence Kinesin-Based Transport In Vitro. Biophys J. 2016; 110:2229–2240. [PubMed: 27224488]

Luo S, Wehr NB, Levine RL. Quantitation of protein on gels and blots by infrared fluorescence of Coomassie blue and Fast Green. Anal Biochem. 2006; 350:233–238. [PubMed: 16336940]

Mandelkow E, Mandelkow EM. Kinesin motors and disease. Trends Cell Biol. 2002; 12:585–591. [PubMed: 12495847]

Maurer SP, Bieling P, Cope J, Hoenger A, Surrey T. GTPgammaS microtubules mimic the growing microtubule end structure recognized by end-binding proteins (EBs). Proc Natl Acad Sci USA. 2011; 108:3988–3993. [PubMed: 21368119]

McKenney RJ, Huynh W, Vale RD, Sirajuddin M. Tyrosination of alpha-tubulin controls the initiation of processive dynein-dynactin motility. EMBO J. 2016; 35:1175–1185. [PubMed: 26968983]

McVicker DP, Chrin LR, Berger CL. The nucleotide-binding state of microtubules modulates kinesin processivity and the ability of Tau to inhibit kinesin-mediated transport. J Biol Chem. 2011; 286:42873–42880. [PubMed: 22039058]

Morikawa M, Yajima H, Nitta R, Inoue S, Ogura T, Sato C, Hirokawa N. X-ray and Cryo-EM structures reveal mutual conformational changes of Kinesin and GTP-state microtubules upon binding. EMBO J. 2015; 34:1270–1286. [PubMed: 25777528]

Nakata T, Niwa S, Okada Y, Perez F, Hirokawa N. Preferential binding of a kinesin-1 motor to GTP-tubulin-rich microtubules underlies polarized vesicle transport. J Cell Biol. 2011; 194:245–255. [PubMed: 21768290]

Nirschl JJ, Magiera MM, Lazarus JE, Janke C, Holzbaur EL. alpha-Tubulin Tyrosination and CLIP-170 Phosphorylation Regulate the Initiation of Dynein-Driven Transport in Neurons. Cell Rep. 2016; 14:2637–2652. [PubMed: 26972003]

Norris SR, Soppina V, Dizaji AS, Schimert KI, Sept D, Cai D, Sivaramakrishnan S, Verhey KJ. A method for multiprotein assembly in cells reveals independent action of kinesins in complex. J Cell Biol. 2014; 207:393–406. [PubMed: 25365993]

Ori-McKenney KM, Xu J, Gross SP, Vallee RB. A cytoplasmic dynein tail mutation impairs motor processivity. Nat Cell Biol. 2010; 12:1228–1234. [PubMed: 21102439]

Rai A, Pathak D, Thakur S, Singh S, Dubey AK, Mallik R. Dynein clusters into lipid microdomains on phagosomes to drive rapid transport toward lysosomes. Cell. 2016; 164:722–734. [PubMed: 26853472]

Rai AK, Rai A, Ramaiya AJ, Jha R, Mallik R. Molecular adaptations allow dynein to generate large collective forces inside cells. Cell. 2013; 152:172–182. [PubMed: 23332753]

Rogers AR, Driver JW, Constantinou PE, Kenneth Jamison D, Diehl MR. Negative interference dominates collective transport of kinesin motors in the absence of load. Phys Chem Chem Phys. 2009; 11:4882–4889. [PubMed: 19506763]

Ruhnow F, Zwicker D, Diez S. Tracking single particles and elongated filaments with nanometer precision. Biophys J. 2011; 100:2820–2828. [PubMed: 21641328]

Sato-Yoshitake R, Yorifuji H, Inagaki M, Hirokawa N. The phosphorylation of kinesin regulates its binding to synaptic vesicles. J Biol Chem. 1992; 267:23930–23936. [PubMed: 1429730]

Schroer TA, Sheetz MP. Two activators of microtubule-based vesicle transport. J Cell Biol. 1991; 115:1309–1318. [PubMed: 1835460]

Seeger MA, Rice SE. Microtubule-associated protein-like binding of the kinesin-1 tail to microtubules. J Biol Chem. 2010; 285:8155–8162. [PubMed: 20071331]

Shubeita GT, Tran SL, Xu J, Vershinin M, Cermelli S, Cotton SL, Welte MA, Gross SP. Consequences of motor copy number on the intracellular transport of kinesin-1-driven lipid droplets. Cell. 2008; 135:1098–1107. [PubMed: 19070579]

Sirajuddin M, Rice LM, Vale RD. Regulation of microtubule motors by tubulin isotypes and post-translational modifications. Nature Cell Biology. 2014; 16:335-+. [PubMed: 24633327]

Sloboda RD, Rosenbaum JL. Purification and assay of microtubule-associated proteins (MAPs). Methods Enzymol. 1982; 85:409–416. [PubMed: 7121279]

Uchimura S, Oguchi Y, Hachikubo Y, Ishiwata S, Muto E. Key residues on microtubule responsible for activation of kinesin ATPase. EMBO J. 2010; 29:1167–1175. [PubMed: 20224548]

Vale RD. The molecular motor toolbox for intracellular transport. Cell. 2003; 112:467–480. [PubMed: 12600311]

Vale RD, Coppin CM, Malik F, Kull FJ, Milligan RA. Tubulin GTP hydrolysis influences the structure, mechanical properties, and kinesin-driven transport of microtubules. J Biol Chem. 1994; 269:23769–23775. [PubMed: 7916345]

Verhey KJ, Gaertig J. The tubulin code. Cell Cycle. 2007; 6:2152–2160. [PubMed: 17786050]

Vershinin M, Carter BC, Razafsky DS, King SJ, Gross SP. Multiple-motor based transport and its regulation by Tau. Proc Natl Acad Sci USA. 2007; 104:87–92. [PubMed: 17190808]

Wang Z, Sheetz MP. The C-terminus of tubulin increases cytoplasmic dynein and kinesin processivity. Biophys J. 2000; 78:1955–1964. [PubMed: 10733974]

Weaver C, Leidel C, Szpankowski L, Farley NM, Shubeita GT, Goldstein LS. Endogenous GSK-3/shaggy regulates bidirectional axonal transport of the amyloid precursor protein. Traffic. 2013; 14:295–308. [PubMed: 23279138]

Wong YL, Rice SE. Kinesin's light chains inhibit the head- and microtubule-binding activity of its tail. Proc Natl Acad Sci U S A. 2010; 107:11781–11786. [PubMed: 20547877]

Xu J, King SJ, Lapierre-Landry M, Nemec B. Interplay between Velocity and Travel Distance of Kinesin-based Transport in the Presence of Tau. Biophysical Journal. 2013; 105:L23–L25. [PubMed: 24268156]

Xu J, Reddy BJ, Anand P, Shu Z, Cermelli S, Mattson MK, Tripathy SK, Hoss MT, James NS, King SJ, et al. Casein kinase 2 reverses tail-independent inactivation of kinesin-1. Nat Commun. 2012a; 3:754. [PubMed: 22453827]

Xu J, Shu Z, King SJ, Gross SP. Tuning multiple motor travel via single motor velocity. Traffic. 2012b; 13:1198–1205. [PubMed: 22672518]

Zhu ZQC, Gupta KK, Slabbekoorn AR, Paulson BA, Folker ES, Goodson HV. Interactions between EB1 and microtubules: Dramatic effect of affinity tags and evidence for cooperative behavior. J Biol Chem. 2009; 284:32651–32661. [PubMed: 19778897]

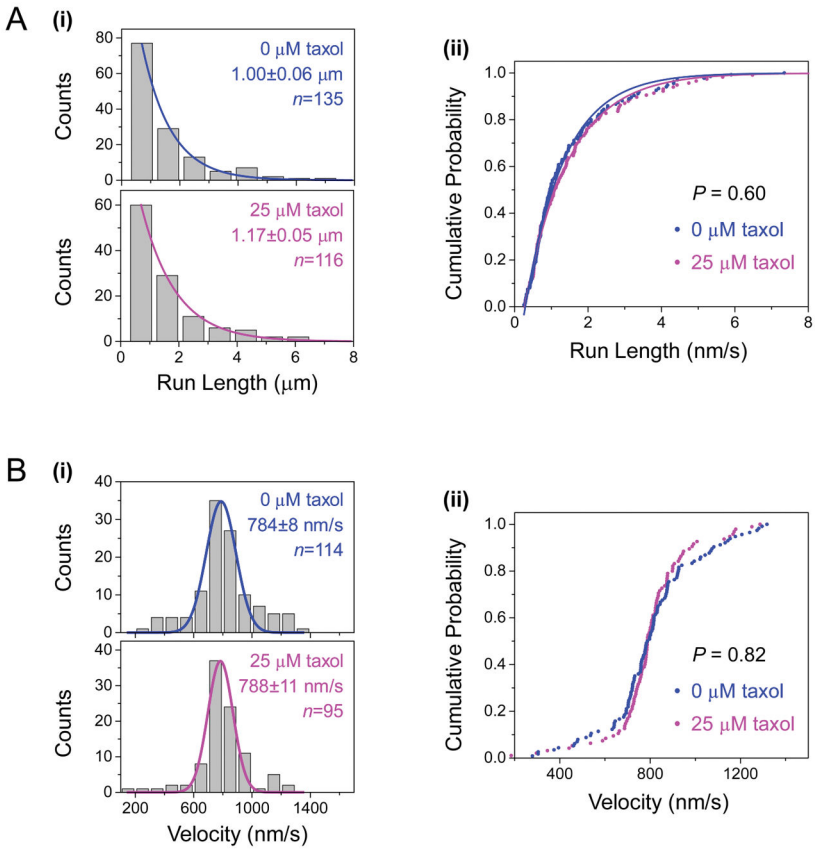

Figure 1. The presence of taxol in motility experiments does not influence the motility of multiple-kinesin cargos along GMPCPP microtubules

GMPCPP microtubules were assembled in the absence of taxol. Taxol concentrations during motility experiments are indicated. (A) Histograms (i) and cumulative probability distributions (ii) of cargo run length along GMPCPP microtubules, in the presence (blue) and the absence (magenta) of taxol. Solid lines, best fits to a single exponential distribution, $e^{-x/d}$. Mean run length (d ± standard error) sample size (n) are indicated. The run length distributions do not differ significantly from each other (P = 0.60, rank-sum test). (B) Histograms (i) and cumulative probability distributions (ii) of cargo velocity along GMPCPP microtubules, in the presence (blue) and absence (magenta) of taxol. Solid lines, best fits to a Gaussian distribution. Mean velocity (± standard error) and sample size (n) are indicated. The velocity distributions do not differ significantly from each other (P = 0.82, Student's t-test).

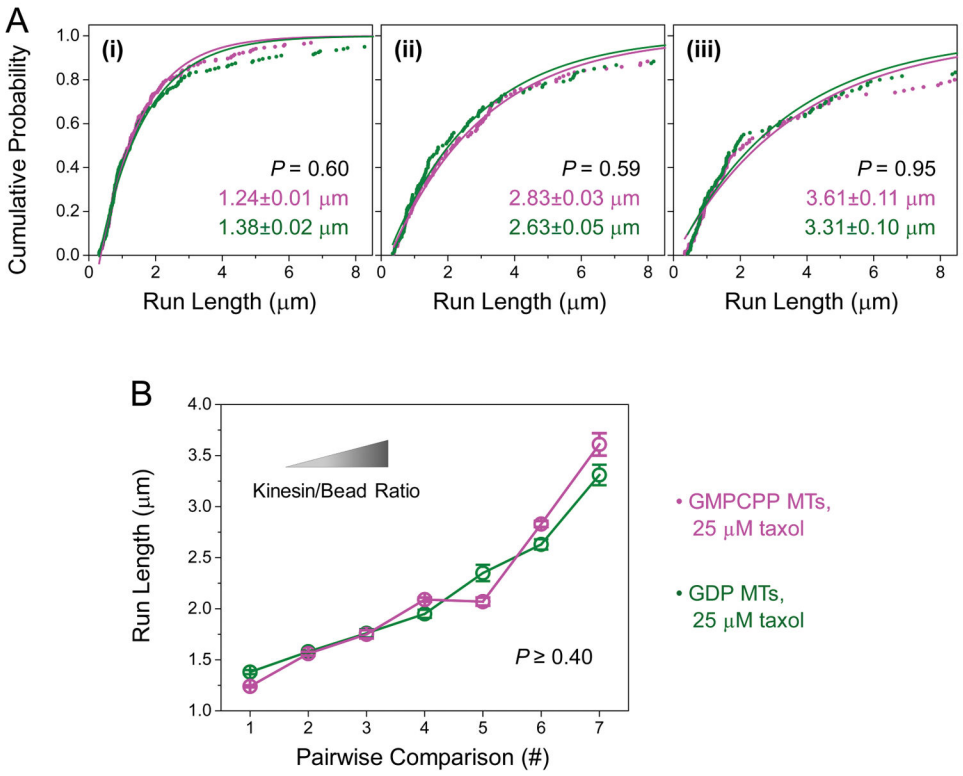

Figure 2. The run length of multiple-kinesin cargos does not differ significantly between GMPCPP and GDP microtubules (MTs)

Taxol (25 μM) was present in buffers during motility experiments for both MT types. (A) Cumulative probability distributions of the run length of multiple-kinesin cargos, shown for three kinesin/bead ratios. Solid lines, best fits to $1\text{-}Ae^{-x/d}$. Mean run length (d ± standard error) and P-value (rank-sum test) are indicated (n = 119–222). (B) Average run length of multiple-kinesin cargos (± standard error), measured for seven kinesin/bead ratios (n = 89–222). Pairwise comparisons #1, #4, and #7 correspond to run-length measurements in (i), (ii), and (iii) of panel (A). The distributions in each set of pairwise comparisons do not differ significantly from each other ($P \geq 0.40$, rank-sum test).

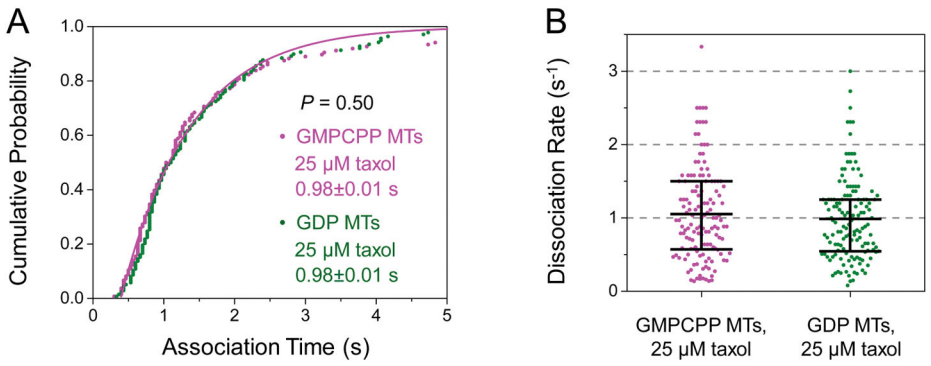

Figure 3. The dissociation rate of a single kinesin does not differ significantly between GMPCPP and GDP microtubules (MTs)

Taxol (25 μM) was present in buffers during motility experiments for both MT types. (A) Cumulative probability distributions of the association time of single kinesins with GMPCPP MTs (n = 136) and GDP MTs (n = 138). Solid lines, best fits to 1-$Ae^{-x/t}$. Mean association time (t ± standard error) is indicated. The two best-fit solid lines share the same average association time and thus overlap with each other. These distributions do not differ significantly from each other (P = 0.50, rank-sum test). (B) Dot plot of single-kinesin dissociation rate for each microtubule type, calculated as the reciprocal of the association time in (A). Horizontal bars indicate mean values and quartiles. These two distributions do not differ significantly from each other (P = 0.50, rank-sum test).

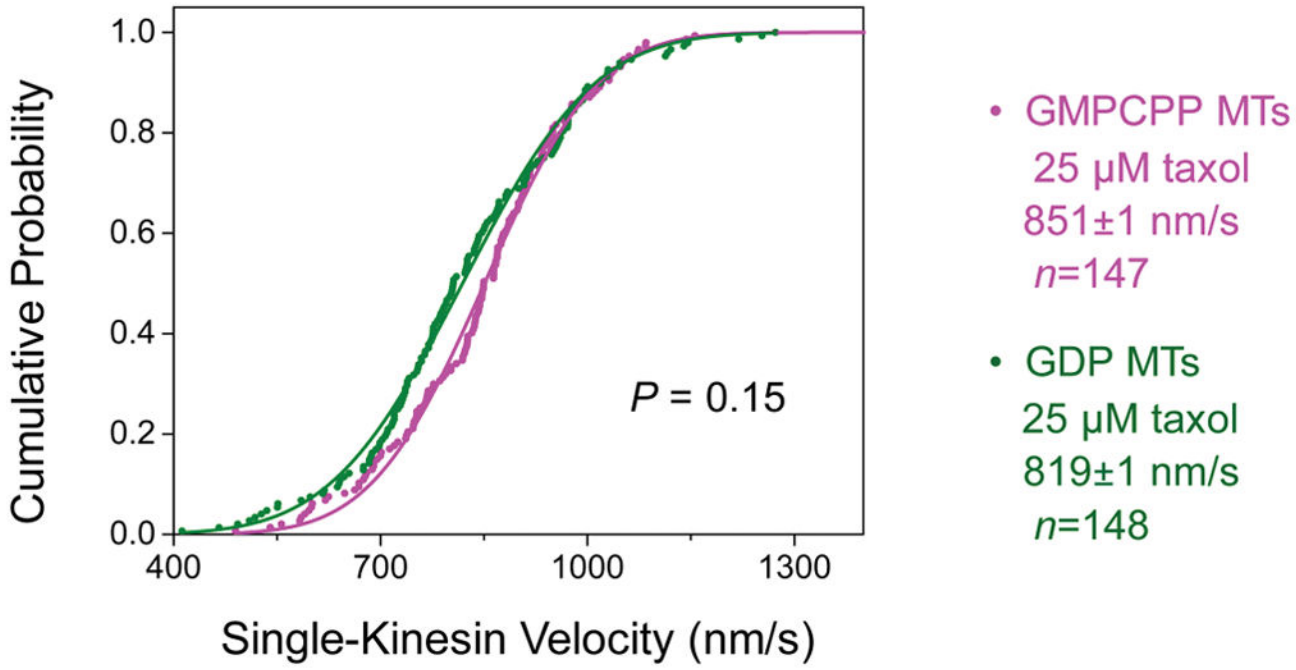

Figure 4. The velocity of single-kinesin cargos does not differ significantly between GMPCPP and GDP microtubules (MTs)

Taxol (25 μM) was present in motility measurements for both MT types. Solid lines, best fits to the cumulative probability distribution of a Gaussian distribution. Mean velocity (± standard error) and sample size (*n*) are indicated. These two distributions do not differ significantly from each other ($P = 0.15$, Student's *t*-test).

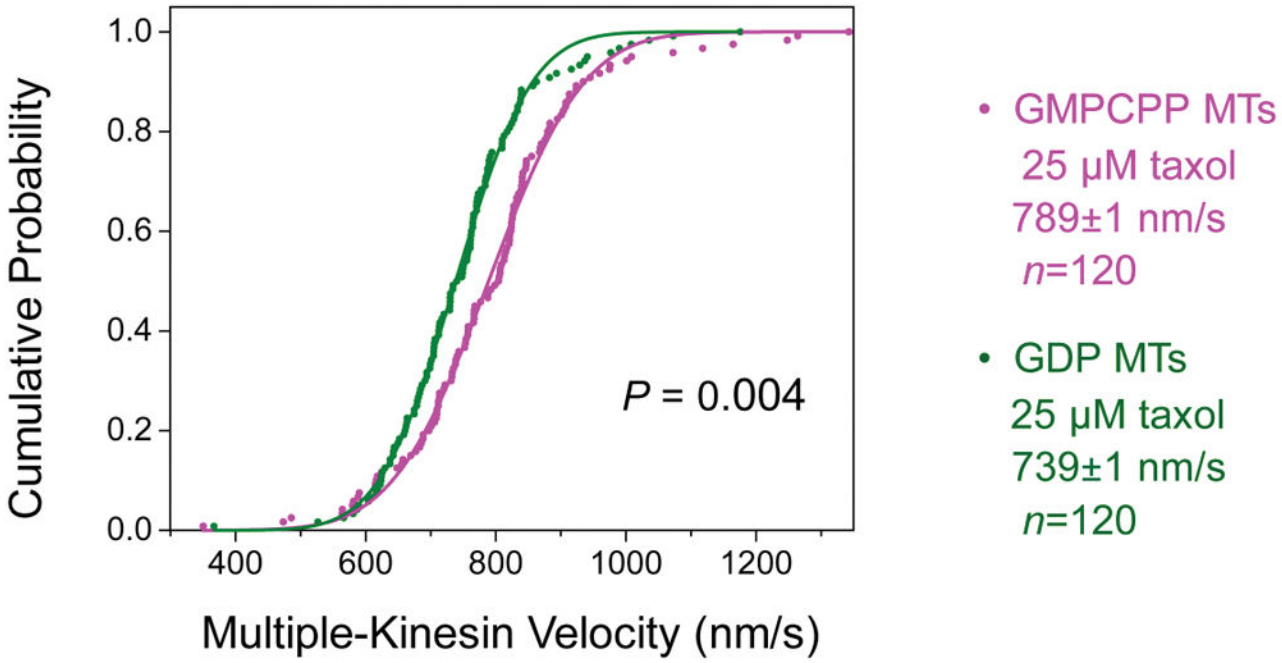

Figure 5. The velocities of multiple-kinesin cargos have a significant but small difference between GMPCPP and GDP microtubules (MTs)

Taxol (25 μM) was present in motility measurements for both MT types. These velocity measurements correspond to run-length measurements in Figure 2A(iii). Solid lines, best fits to the cumulative probability distribution of a Gaussian distribution. Mean velocity (± standard error) and sample size (*n*) are indicated. For both MT types, the velocities of multiple-kinesin cargos are somewhat lower than that of single-kinesin cargos shown in Figure 4. This reduction in velocity with increasing motor number per cargo is consistent with recent in vitro findings by ourselves [Xu et al., 2013] and others [Conway et al., 2012]. Mean velocity of multiple-kinesin cargos was 1.07× faster on GMPCPP MTs than on GDP MTs ($P = 0.004$, Student's *t*-test).

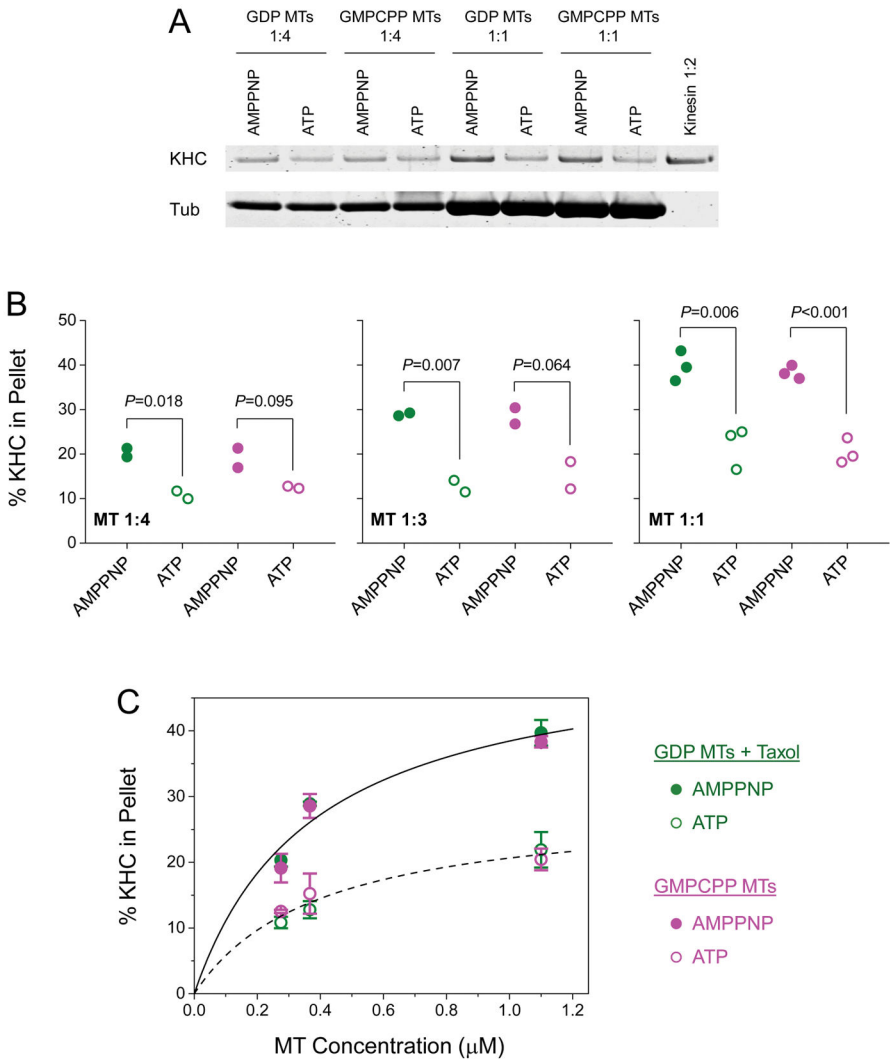

Figure 6. Native kinesin-1 does not preferentially co-sediment with GTP-tubulin-rich microtubules (MTs)

Co-sedimentation was measured using bead-independent MT-affinity pulldown assays. Taxol (25 μM) was included in assays using GDP MTs. Assays using GMPCPP MTs were free of taxol. (A) Example co-sedimentation assays at two microtubule concentrations (1:1 and 1:4, corresponding to 0.28 and 1.1 μM MT, respectively), and in the presence of 5 mM AMPPNP or 5 mM ATP as indicated. KHC, kinesin heavy chain; Tub, tubulin. Dilution of kinesin reference solution (1:2) corresponds to 50% of the input kinesin. The un-cropped image of this gel is shown in Figure S4. (B) Dot plot of the fraction of KHC signal in the MT pellet, measured for three MT concentrations (1:4, 1:3, and 1:1; corresponding to 0.28, 0.37, and 1.1 μM MT, respectively). Green solid (or open) circle, assays using taxol-stabilized GDP MTs at 5 mM AMPPNP (or 5 mM ATP). Magenta solid (or open) circle, assays using taxol-free GMPCPP MTs at 5 mM AMPPNP (or 5 mM ATP). *P*-value is determined using Student's *t*-test. (C) Mean and standard error of KHC measurements in (B), as a function of MT concentration. Solid line, best fit of KHC signal in the presence of

AMPPNP (averaged between MT types) to the Hill equation. Dashed line, best fit of KHC signal in the presence of ATP (averaged between MT types) to the Hill equation.